ACS APPLIED MATERIALS & INTERFACES

RESEARCH ARTICLE

www.acsami.org

Indium Tin Oxide Nanorod Electrodes for Polymer Photovoltaics

Man Kin Fung,[†] Ye Chuan Sun,[†] Annie Ng,[†] Alan Man Ching Ng,[†] Aleksandra B. Djurišić,[*,†] Hung Tat Chan,[‡] and Wai Kin Chan[‡]

[†]Department of Physics and [‡]Department of Chemistry, The University of Hong Kong, Pokfulam Road, Hong Kong

ABSTRACT: We have deposited indium tin oxide (ITO) nanorods on glass and glass/ITO substrates by DC sputtering and by e-beam deposition. The properties of the nanorods deposited by different methods and on different substrates have been investigated. The ITO nanorods were also used as an electrode in bulk heterojunction polymer solar cells. We found that the nanorod morphology and sheet resistance had a significant effect on the solar cell performance, with significant improvements in the efficiency compared to commercial ITO film substrates in all cases except for e-beam deposited nanorods on glass that had high sheet resistance. The best power conversion efficiency achieved was 3.2 % (for sputtered ITO nanorods on ITO), compared to 2.1 % for commercial ITO substrates.

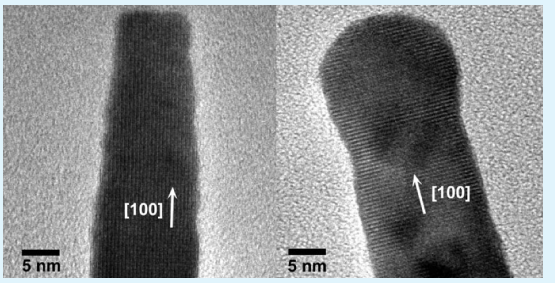

KEYWORDS: indium tin oxide, nanorods, e-beam deposition, sputtering, polymer solar cells, bulk heterojunction solar cells

1. INTRODUCTION

Polymer solar cells are of significant interest as promising candidates for low-cost photovoltaics.[1−25] Although major research effort is devoted to the development of novel materials for polymer photovoltaics, in recent years there have also been increasing attempts to improve the device performance by optimizing the device architecture to improve light trapping and/or charge collection.[5−14] Because poly(3-hexylthiophene):1-(3-methoxycarbonyl)-propyl-1-phenyl-(6,6)C_{61} (P3HT:PCBM) bulk heterojunction is the most commonly investigated material combination,[1−4,15−21,23,24] and it achieves reasonably high efficiency (typically between 2.7 and 5.0%,[1] although lower efficiencies such as 1.3%[7] have also been reported), the majority of the efforts to optimize the device architecture[5−7,11−14] have been concentrating on this material system. For example, to improve the performance of the devices, imprinting the P3HT:PCBM active layer with grating structures,[5,6] textured rough surfaces,[7] and anodized alumina[10] has been performed. The improvement was attributed to increased surface roughness and light trapping,[5−7,10] although improved P3HT ordering after imprinting[7,10] may also play a role in the observed performance improvements. Other reported methods for texturing the active layer surface are pattern replication in non-wetting templates,[8] porous film preparation by blending an additive,[11] and surface texturing by conductive atomic force microscopy (C-AFM).[12]

In addition to increasing the light trapping by active layer texturing, performance can be also enhanced by improving the charge collection. For example, the fabrication of P3HT nanostructures by imprinting P3HT with anodized alumina was reported, and the improvement in the performance of such P3HT/C_{60} cells has been attributed to improved charge separation.[9] Texturing of the active blend layer can also result in improved charge collection due to larger interface between the active layer and the electrode.[11] Alternative approach to texturing of the active layer is the incorporation of inorganic nanorods into the active layer to achieve improved charge collection.[13,14] For P3HT:PCBM, this approach has been successfully demonstrated with ZnO nanorods[13] and indium tin oxide (ITO) nanorods.[14] ITO nanorods were deposited on ITO films by oblique angle e-beam deposition.[14] This technique has been demonstrated for successful preparation of ITO nanorod arrays for applications as antireflective coatings[26,27] and structures for improving the light extraction from nitride-based light emitting diodes.[28] In this deposition method, the substrate is tilted at an angle of 70° .

In this work, we have prepared ITO nanorods by two different methods, sputtering and electron-beam (e-beam) deposition. For both methods, the deposition time was very short and the nanorods could be grown without tilting the substrate, resulting in a simple and fast nanorod growth. ITO nanorod deposition by both methods has been demonstrated on glass substrates and ITO film/glass substrates. Different substrates with ITO nanorods have been applied in bulk heterojunction solar cells with P3HT:PCBM (1:1) blend active layer. Improvements in device performance are observed in all cases except ITO nanorods deposited by e-beam on glass, because of their high sheet resistance. The relationship between ITO nanorod properties and solar cell performance is discussed.

2. EXPERIMENTAL SECTION

ITO Nanorod Growth and Characterization. ITO (Varitronix Ltd) and glass substrates were ultrasonically cleaned in

Received: November 11, 2010
Accepted: January 26, 2011
Published: February 7, 2011

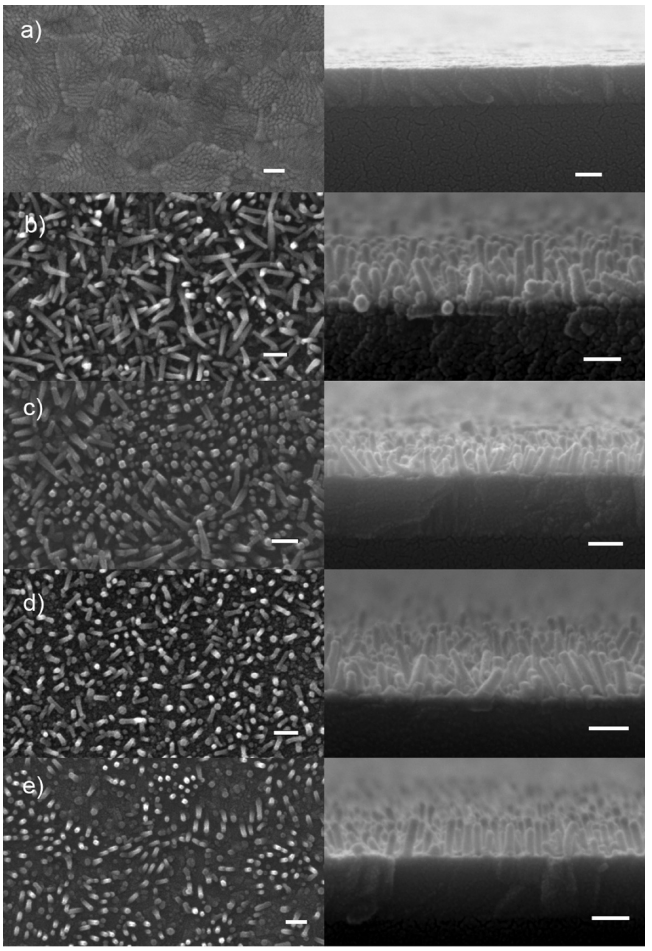

Figure 1. Top view (left) and cross-section (right) SEM images of (a) C-ITO, (b) E/glass, (c) E/ITO, (d) S/glass, (e) S/ITO samples. The scale bar in all images is 100 nm.

toluene, acetone, ethanol and deionized water for 5 minutes each. The samples were then dried in nitrogen flow before exposure to UV ozone for 5 minutes. The ITO rods were fabricated by two methods, namely the e-beam evaporation and DC sputtering, using an Advanced System Technology (AST) Peva-400ES deposition system equipped with an e-beam deposition and a sputter gun. Indium oxide/tin dioxide (90/10 wt %) pieces (Kurt J. Lesker Company, purity of 99.99%) were used as the source. The substrates were placed on a rotating sample holder at a distance 9 cm from the center of rotation. The working pressure of the chamber was kept at $7x10^{-6}$ Torr and the substrates were heated up to 350 °C. The deposition was then performed for a specified time (typically ~4 min.) to achieve the nanorod length in the range ~150−200 nm. For sputtered ITO nanorods, base pressure in the chamber and the substrate temperature were the same, but the substrates were not rotating. The vertical distance between the In_2O_3/ SnO_2 (90/10 wt %) target (ProTech Materials, purity: 99.99%) and the sample holder was 14 cm. After introducing Ar gas at a flow rate of 19 sccm, samples were sputtered at fixed current (0.7 A) for 1 min. Both e-beam deposition and sputtering were performed without introducing oxygen gas into the chamber.

The sheet resistances were measured using a four-point probe with a Keithley 2400 sourcemeter. Optical transmittance measurements were carried out using a Cary 50 Bio UV- vis spectrophotometer. The morphologies of the ITO samples were examined using a JEOL JSM-7001F field emission scanning electron microscope (SEM) and transmission electron microscopy (TEM) and selected area electron

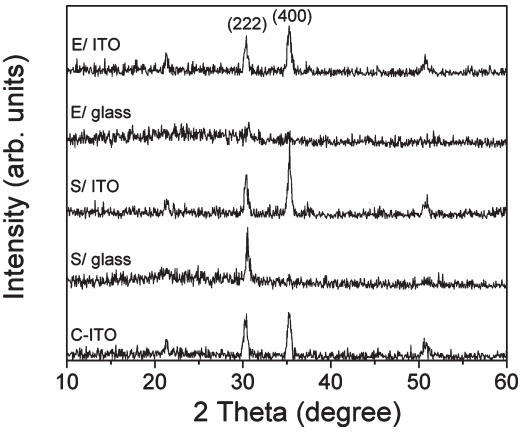

Figure 2. XRD patterns of different ITO samples. The curves have been shifted for clarity and the main diffraction peaks are labeled.

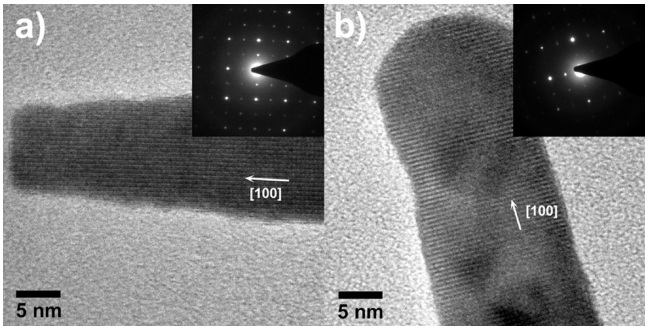

Figure 3. TEM images of nanorods from (a) E/ITO and (b) S/ITO samples. Growth directions are indicated by arrows. The insets show corresponding SAED patterns.

diffraction (SAED) with a Tecnai G2 20 S-Twin. X-ray diffraction (XRD) measurements were performed using a Bruker AXS SMART CCD diffractometer. SEM was also used for imaging the cross-section of the device structures after breaking the samples (in liquid nitrogen for complete devices and ambient for poly(3,4-ethylene-dioxythiophene)/ poly(styrenesulfonate) (PEDOT:PSS) only), followed by sputtering a thin layer of Au. Thickness of the polymer films was determined from the cross-section SEM images as an average of 5 points.

Solar Cells. The ITO samples were first cleaned with UV ozone treatment for 5 minutes. As-received PEDOT:PSS (Clevios P VP AI 4083) solution was passed through a 0.45 μm filter and spin-coated at 5000 rpm for 2 minutes. The substrates were dried in a vacuum oven at 120 °C for 20 minutes. For the active layer, 40 mg/mL poly-(3-hexylthiophene) (P3HT) in chlorobenzene and a solution of 40 mg/mL [6,6]-phenyl-C61-butyric acid methyl ester (PCBM) in chlorobenzene were prepared separately. They were stirred in nitrogen atmosphere at 40 °C for 18 h. Both solutions were mixed for 3 h before use. The mixed solution was then passed through a 0.45 μm filter and spin-cast on top of the PEDOT:PSS layer at 500 rpm for 1 min. 100 nm Al was thermally evaporated on the active layer as the top electrode in high vacuum. The active area of the cells was 3.14 mm^2. Finally, the completed devices were annealed at 130 °C for 5 minutes under nitrogen atmosphere. Topography and surface roughness of the samples were characterized by atomic force microscopy (AFM) using a Asylum Research MFP-3D in tapping mode (with a silicon tip coated with Al reflective coating, force constant of 2 N/m and resonance frequency of 70 kHz). The I−V characteristics were measured with a Keithley 2400 sourcemeter in ambient. ABET Technologies Sun 2000 Solar Simulator with an AM1.5 filter was used as light source. The power density was

Table 1. Substrate Sheet Resistance (average value of three substrates) and Solar Cell Performance Parameters[a]

	V_{oc} (V)	J_{sc} (mA/cm^2)	FF	eff (%)	R_s (ohm/sq)
C-ITO	0.57 ± 0.004 (0.58)	7.1 ± 0.6 (7.8)	0.44 ± 0.01 (0.45)	1.8±0.2 (2.1)	14
S/glass	0.57 ± 0.01 (0.57)	8.4 ± 0.8 (9.8)	0.46 ± 0.04 (0.49)	2.3 ± 0.4 (2.8)	166.7
S/ITO	0.57 ± 0.004 (0.57)	9.0 ± 0.8(10.2)	0.51 ± 0.02 (0.55)	2.6 ± 0.3 (3.2)	12.2
E/glass	0.56 ± 0.01 (0.58)	7.1 ± 0.8 (8.4)	0.38 ± 0.04 (0.43)	1.5 ± 0.3 (2.1)	563.8
E/ITO	0.57 ± 0.01 (0.58)	8.2 ± 0.8 (9.0)	0.50 ± 0.01 (0.52)	2.4 ± 0.3 (2.7)	13.1

[a] In each case, three substrates prepared on different days were considered, and the number of devices per substrate was 6 for C-ITO and 3 for other substrates. In addition to the average value, the best obtained result is given in brackets.

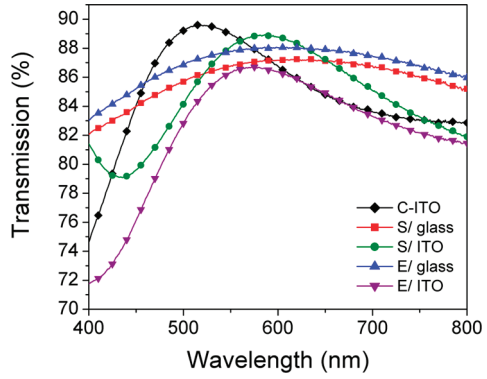

Figure 4. Transmission of different ITO samples. Diamonds denote C-ITO, squares denote S/glass, circles correspond to S/ITO, whereas up and down triangles denote E/glass and E/ITO samples, respectively.

measured by a Molectron Power Max 500D power meter and adjusted to 100 mW cm^{-2}. The external quantum efficiency (EQE) was measured after I−V curve measurements under ambient conditions using an Oriel 66002 solar simulator and a Thermo Oriel 257 monochromator for monochromatic illumination of the devices, whereas photocurrents and the light intensity were measured using a Keithley 2400 sourcemeter and a Newport 1830-C power meter with an 818-UV detector probe, respectively.

3. RESULTS AND DISCUSSION

Figure 1 shows the SEM images (top view and side view) of commercial ITO film (C-ITO), and ITO nanorods prepared by e-beam (E/glass and E/ITO) and sputtering (S/glass and S/ITO) on glass and ITO substrates. It can be observed that both e-beam deposition and sputtering result in a similar nanorod dimensions and morphology. In terms of the substrate, the orientation of the nanorods is improved for ITO substrates as compared to glass. XRD measurements have also been performed to characterize the nanorods and the obtained patterns are shown in Figure 2. It can be observed that for nanorods grown on glass the dominant peak is (222), while for those grown on ITO films both (222) and (400) peaks can be observed, with (400) peak having a higher intensity compared to the ITO film substrate (JCPDS file No. 89-4598). To examine the nanorods in more detail, TEM has been performed. Representative TEM images with a corresponding SAED pattern for nanorods grown by e-beam deposition and sputtering are shown in Figure 3. It can be observed that the growth direction is the same for both deposition methods, in agreement with the fact that [100] growth direction is commonly observed in ITO and In_2O_3 1D nanostructures.[29] Unlike ITO nanorods grown by oblique deposition,[27,28] no core−shell structures were observed.

Concerning the growth mechanism of ITO nanorods, because no metal catalysts were used, nanorods could form either because of vapor−solid or self-catalyzed vapor−liquid−solid (VLS) mechanism. It was proposed that the ITO nanorod growth during oblique e-beam deposition with a nitrogen flux occurs because of self-catalytic vapor−liquid−solid (VLS) method, where tin-doped indium nuclei readily form in an oxygen deficient environment.[26] In our deposition methods, the environment is also oxygen deficient since no oxygen gas was introduced during deposition, and it was proposed that catalytic particles for self-catalytic VLS growth can readily form for low melting point metals,[30] which would be the case for indium and tin. Therefore, self-catalytic VLS mechanism is a likely growth mechanism for these nanowires. This is also supported by the fact that some of the nanorods exhibit rounded particle-like structures (see Figure. 3b), which have the same lattice spacing as the body of the nanorod. If the growth was a self-catalytic VLS, the oxidation of the catalytic indium−tin particle would result in the structure which has been observed in the TEM.

For device applications of these nanorods, transmittance and sheet resistance are very significant. The sheet resistances are summarized in Table 1, whereas Figure 4 shows the transmittance of different ITO samples. It can be observed that the transmittances of ITO nanorods on glass are better than that of commercial ITO film (except in a very narrow range), but the sheet resistances are significantly higher for both E/glass and S/glass samples. Similar improvement in the transmittance of ITO nanorods compared to ITO film has been previously observed.[28] However, in our case, transmittance of ITO nanorods on ITO film is slightly lower compared to ITO film for wavelengths below 600 nm, especially for E/ITO sample. Because the transmittance and sheet resistance of ITO are typically dependent on its stoichiometry, i.e., incorporation of oxygen,[26] it is possible that there are differences in the stoichiometry which contribute to lower transmittance of these films. In addition, the substrate used can also affect the transmittance of the deposited ITO,[31−33] which can occur because of differences in oxygen incorporation,[31,32] microstructure,[31] or surface roughness, leading to different scattering losses.[33] From the SEM images and XRD patterns, we can observe differences in degree of orientation of the nanorods deposited by two methods on glass and ITO substrates, which in addition to possible small composition and thickness variations may result in observed differences in the transmission. The sheet resistance of S/ITO and E/ITO samples is somewhat lower compared to the bare ITO film, whereas the samples deposited on glass had significantly higher sheet resistance, especially in the case of E/glass samples.

Different ITO substrates were used in bulk heterojunction solar cells. To characterize the film quality and polymer

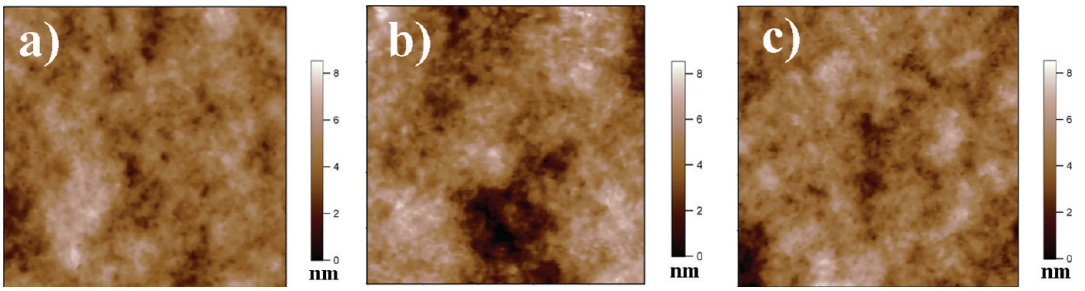

Figure 5. AFM images of active P3HT:PCBM layer spin-coated on top of PEDOT:PSS on (a) C-ITO, (b) S/ITO, (c) E/ITO.

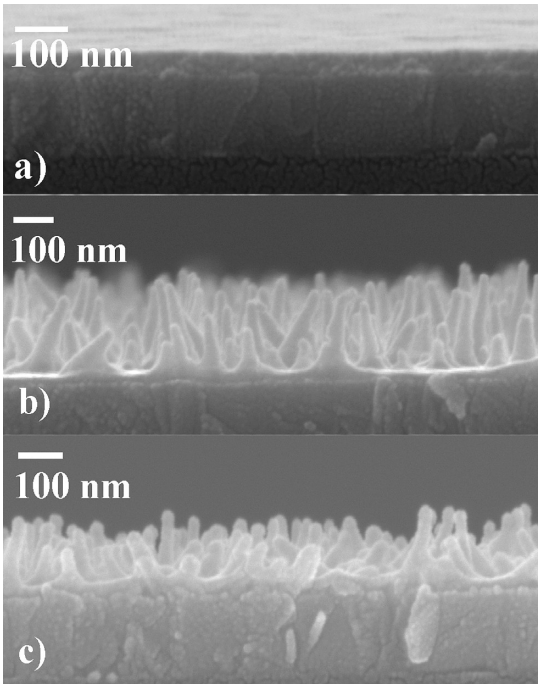

Figure 6. Cross-section SEM images of PEDOT:PSS spin-coated on (a) C-ITO, (b) S/ITO, (c) E/ITO.

infiltration, AFM and cross-section SEM imaging was performed. Representative AFM images are shown in Figure 5. It can be observed that the morphology of the films is similar in all cases. The rms roughness values are also similar for all substrates, with only a small increase for S/ITO substrates, 0.9 nm for C-ITO, 1.0-1.1 nm for E/glass, 1.0 nm for E/ITO, 0.9 nm for S/glass, and 1.4 nm for S/ITO. To examine the infiltration of the polymer and determine the polymer layer thickness, cross-section SEM imaging has been performed. PEDOT:PSS layer on ITO film and ITO nanorods deposited by two different methods is shown in Figure 6. The PEDOT:PSS thickness is ~40 nm, and it can be observed that PEDOT:PSS conformally covers the ITO nanorods. From the device cross-section images shown in Figure 7, good infiltration of the polymer can be observed in all cases. The active layer thickness (obtained by subtracting the PEDOT:PSS thickness from the total polymer thickness) is ~260 nm for C-ITO, ~280 nm for E/glass and S/glass substrates, ~335 nm for E/ITO, and ~315 nm for S/ITO. The increased thickness for substrates with nanorods is likely due to the change in the wetting properties because of nanostructured morphology.

It should be noted that the film thickness in our work is relatively high, in order to prevent short circuit and electrode

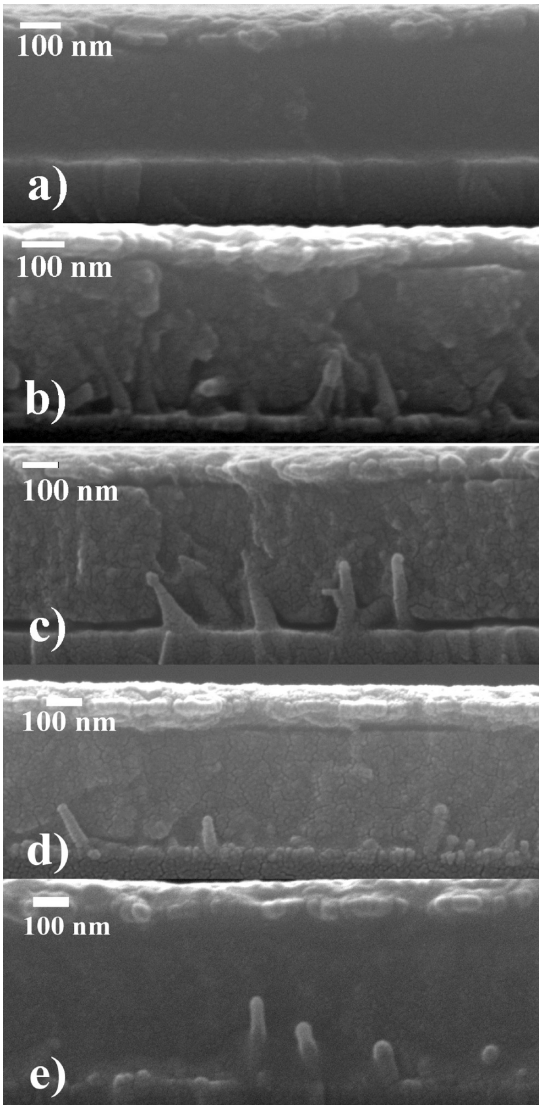

Figure 7. Cross-section SEM images of solar cell devices on (a) C-ITO, (b) S/glass, (c) S/ITO, (d) E/glass, and (e) E/ITO. The scale bars are 100 nm.

proximity effects (electrode proximity effects could result in the reduction of FF[14]). Higher thickness results in overall lower efficiency of the cells compared to an optimal P3HT:PCBM thickness for planar devices. Several solar cell performance parameters (power conversion efficiency (PCE), J_{sc} and FF) exhibit strong dependence on the active layer thickness.[17,19,21] Although J_{sc} typically exhibits oscillating dependence on the

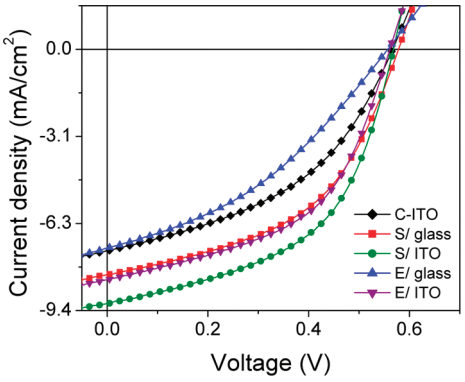

Figure 8. Representative (close to average) $I-V$ curves of solar cells on different ITO substrates. Diamonds denote C-ITO, squares denote S/glass, circles correspond to S/ITO, whereas up and down triangles denote E/glass and E/ITO samples, respectively.

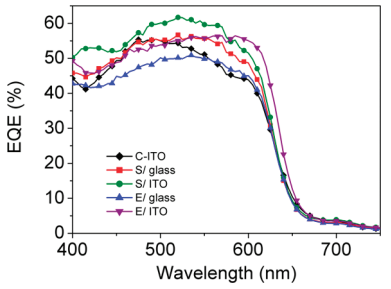

Figure 9. Representative EQE curves of solar cells on different ITO substrates. Diamonds denote C-ITO, squares denote S/glass, circles correspond to S/ITO, whereas up and down triangles denote E/glass and E/ITO samples, respectively.

active layer thickness due to optical interference effects,[17,19] FF decreases with increasing thickness[17,21] because of increased recombination losses[17,21] and increased resistance of the active layer.[21] In addition, even for the same film thickness, spin-coating from a more concentrated solution results in lowering of the overall efficiency.[16] However, in devices containing nanorods primary consideration in device fabrications is that the polymer is well-infiltrated and the rods are fully covered. Thus, we tried different preparation conditions for the active layer. To achieve thinner layers, spin-coating from a less concentrated solution (30 mg/mL) was performed. This results in an active layer thickness of ~160 nm, which results in the efficiency of ~1.4−1.5% for C-ITO, 1.6-1.7 % for E/glass and ~2.1% for E/ITO. However, for this device thickness, all S/glass and S/ITO devices exhibited short-circuit (likely due to somewhat longer length of sputtered nanorods). Solution concentration of 20 mg/mL did not result in reproducible working devices for substrates with nanorods.

Therefore, we concentrated on devices prepared with solution concentration of 40 mg/mL. Obtained solar cell performance parameters are summarized in Table 1, and $I-V$ curves are shown in Fig. 8. It can be observed that for all samples except E/glass the photovoltaic performance is improved. In particular, short circuit current density and fill factor are improved compared to devices fabricated on ITO film. Improvement in the efficiency due to increase in both J_{sc} and FF[11] or just the FF[14] indicate improved charge collection. In previous report of P3HT:PCBM cells with ITO nanorod electrodes, an increase in the short circuit current density and a decrease in the fill factor was reported.[14] The increase in J_{sc} was attributed to improved charge collection, whereas the decrease in fill factor was attributed to decreased shunt resistance, possibly due to the proximity of nanorods to the Al electrode.[14] From cross-section SEM images (Figure 7), we can observe good infiltration of the polymer and sufficient separation between the top electrode and nanorods, so that an improvement in the charge collection would be expected. Differences in the active layer thickness may also contribute to the observed performance differences. However, thicker layers are expected to result in decreased FF value,[17] whereas we observed an increase in FF for S/ITO and E/ITO in spite of the increased film thickness. Small reduction in the substrate sheet resistance for these samples is unlikely to be sufficient reason for the observed FF increase. Therefore, we can conclude that observed performance improvements are most likely due to an improved charge collection. FF and J_{sc} exhibited a decrease for E/glass samples, likely due to high sheet resistance of those samples. S/ITO samples exhibited better performance compared to E/ITO samples, which is likely due to higher transmittance of S/ITO substrates. The S/glass samples exhibited comparable performance to E/ITO samples and improved performance compared to C-ITO samples, in spite of significantly higher sheet resistance. Consequently, S/glass exhibited lower FF value compared to E/ITO, but higher FF value compared to C-ITO, which is an indication of improved charge collection. Thus, sputtering of ITO nanorods results in an improved performance compared to e-beam nanorod deposition. For both deposition methods, deposition on ITO rather than on glass results in improved performance due to significantly lower sheet resistance. For substrates with similar nanorod morphology and similar sheet resistance (S/ITO and E/ITO), the photovoltaic performance is then affected by the substrate transmission, so that S/ITO, which has higher transmission, exhibits better performance. To characterize photovoltaic performance of the devices in more detail, EQE measurements were performed and the obtained results are shown in Figure 9. Because the interfaces in devices are not planar, internal quantum efficiency could not be estimated. The differences in the EQE curves are partly due to differences in the transmission spectra (i.e., the position of the minimum point between 400-500 nm in S/ITO samples) and partly due to differences in the charge collection efficiency (for example, E/glass has higher transmission but lower EQE compared to S/ITO samples). Thus, we have demonstrated that bulk heterojunction polymer solar cell performance could be improved by introduction of ITO nanorods grown by different methods (e-beam deposition and sputtering) using simple procedures and short deposition times. For further improvements in the device performance, it would be necessary to carefully optimize nanorod length and active layer processing conditions (solution concentration and spin-coating parameters) and annealing treatment (longer annealing time may be beneficial for thicker films[18]).

4. CONCLUSIONS

We have prepared ITO nanorods on glass and ITO substrates by two simple deposition methods, e-beam deposition and sputtering. Different ITO samples were used as substrates for bulk heterojunction polymer solar cells. We found that the ITO nanorods resulted in improved charge collection and

consequently improved photovoltaic performance. However, sample structure and deposition conditions which resulted in high substrate sheet resistance did not result in significant improvements in charge collection. For comparable electrical properties and morphology of the substrates, higher transmittance resulted in higher power conversion efficiency. The best efficiency achieved for sputtered ITO nanorods on ITO film was 3.2%, which was significantly higher compared to 2.1% achieved for bare ITO film.

AUTHOR INFORMATION

Corresponding Author

*Tel: +852 2859 7946. Fax: +852 2559 9152. E-mail: dalek@hku.hk.

ACKNOWLEDGMENT

Financial support from the Strategic Research Theme, University Development Fund, and Small Project Funding of the University of Hong Kong is acknowledged. The authors thank Prof. M. H. Xie for useful discussions.

REFERENCES

(1) Dennler, G.; Scharber, M. C.; Brabec, C. J. *Adv. Mater.* **2009**, *21*, 1323–1338.
(2) Li, G.; Yao, Y.; Yang, H.; Shrotriya, V.; Yang, G.; Yang, Y. *Adv. Funct. Mater.* **2007**, *17*, 1636–1644.
(3) Wang, W. L.; Wu, H. B.; Yang, C. Y.; Luo, C.; Zhang, Y.; Chen, J. W.; Cao., Y. *Appl. Phys. Lett.* **2007**, *90*, 183512–1-3.
(4) Reyes-Reyes, M.; Kim, K.; Carroll, D. L. *Appl. Phys. Lett.* **2005**, *87*, 083506–1-3.
(5) Na, S.I.; Kim, S. S.; Jo, J.; Oh, S. H.; Kim, J.; Kim, D.Y. *Adv. Funct. Mater.* **2008**, *15*, 3956–3963.
(6) Na, S. I.; Kim., S. S.; Kwon, S. S.; Jang, J.; Kim, J.; Lee, T.; Kim, D. Y. *Appl. Phys. Lett.* **2007**, *91*, 173509–1-3.
(7) Shih, C. F.; Hung, K. T.; Wu, J.W.; Hsiao, C. Y.; Li, W. M. *Appl. Phys. Lett.* **2009**, *94*, 143505–1-3.
(8) Ko, D. H.; Tumbleston, J. R.; Zhang, L.; Williams, S.; DeSimone, J. M.; Lopez, R.; Samulski, E. T. *Nano Lett.* **2009**, *9*, 2742–2746.
(9) Kim, J. S.; Park, Y.; Lee, D. Y.; Lee, J. H.; Park, J. H.; Kim, J. K.; Cho, K. *Adv. Funct. Mater.* **2010**, *20*, 540–545.
(10) Lee, J. H.; Lim, D. W.; Jang, H.; Choi, J. K.; Geng, J. X.; Lung, J. W.; Yoon, S. C.; Jung, H. T. *Small* **2009**, *5*, 2139–2143.
(11) Lee, H. K.; Jeon, J. H.; Wang, D. H.; Park, O. O.; Kim, J. K.; Im, S. H.; Park, J. H. *Appl. Phys. Lett.* **2010**, *96*, 103304–1-3.
(12) Zaniewski, A. M.; Loster, M.; Zettl, A. *Appl. Phys. Lett.* **2009**, *95*, 103308–1-3.
(13) Takanezawa, K.; Tajima, K.; Hashimoto, K. *Appl. Phys. Lett.* **2008**, *93*, 063308–1-3.
(14) Yu, P. C.; Chang, C. H.; Su, M. S.; Hsu, M. H.; Wei, K. H. *Appl. Phys. Lett.* **2010**, *96*, 153307–1-3.
(15) Salim, T.; Wong, L. H.; Brauer, B.; Kukreja, R.; Foo, Y. L.; Bao, Z. N.; Lam, Y. M. *J. Mater. Chem.* **2011**, *21*, 242–250.
(16) Baek, W. H.; Yang, H.; Yoon, T. S.; Kang, C. J.; Lee, H. H.; Kim, Y. S. *Sol. Energy Mater. Sol. Cells* **2009**, *93*, 1263–1267.
(17) Nam, Y. M.; Huh, J.; Jo, W. H. *Sol. Energy Mater. Sol. Cells* **2010**, *94*, 1118–1124.
(18) Jung, J. W.; Jo, W. H. *Appl. Phys. Lett.* **2010**, *97*, 053395–1-3.
(19) Li, G.; Shrotriya, V.; Yao, Y.; Yang, Y. *J. Appl. Phys.* **2005**, *98*, 043704–1-5.
(20) Yun, M. H.; Kim, G. H.; Yang, C.; Kim, J. Y. *J. Mater. Chem.* **2010**, *20*, 7710–7714.
(21) Kim, M. S.; Kim, B. G.; Kim, J. *ACS Appl. Mater. Interfaces* **2009**, *1*, 1264–1269.
(22) Zhao, G. J.; He, Y. J.; Li, Y. F. *Adv. Mater.* **2010**, *22*, 4355–4358.
(23) Reese, M. O.; Nardes, A. M.; Rupert, B. L.; Larsen, R. E.; Olson, D. C.; Lloyd, M. T.; Shaheen, S. E.; Ginley, D. S.; Rumbles, G.; Kopidakis, N. *Adv. Funct. Mater.* **2010**, *20*, 3476–3483.
(24) Verploegen, E.; Mondal, R.; Bettinger, C. J.; Sok, S.; Toney, M. F.; Bao, Z. A. *Adv. Funct. Mater.* **2010**, *20*, 3519–3529.
(25) Lim, B.; Jo, J.; Na, S. I.; Kim, J.; Kim, S. S.; Kim, D. Y. *J. Mater. Chem.* **2010**, *20*, 10919–10923.
(26) Chang, C. H.; Yu, P. C.; Yang, C. S. *Appl. Phys. Lett.* **2009**, *94*, 051114–1-3.
(27) Yu, P. C.; Chang, C. H.; Chiu, C. H.; Yang, C. S.; Yu, J. C.; Kuo, H. C.; Hsu, S. H.; Chang, Y. C. *Adv. Mater.* **2009**, *21*, 1618–1621.
(28) Chiu, C. H.; Yu, P. C.; Chang, C. H.; Yang, C. S.; Hsu, M. H.; Kuo, H. C.; Tsai, M. A. *Opt. Express* **2009**, *17*, 21250–21256.
(29) Ding, G. Q.; Shen, W. Z.; Zheng, M. J.; Zhou, Z. B. *Nanotechnology* **2006**, *17*, 2590–2594.
(30) Kolasinski, K. W. *Curr. Opin. Solid State Mater. Sci.* **2006**, *10*, 182–191.
(31) Wang., R. X.; Beling, C. D.; Djurišić, A. B.; Li, S.; Fung, S. *Semicond. Sci. Technol.* **2004**, *19*, 695–698.
(32) de Carvalho, C. N.; Lavareda., G.; Fortunato, E.; Amaral, A. *Thin Solid Films* **2003**, *427*, 215–218.
(33) Kim, H. J.; Bae, J. W.; Kim, J. S.; Kim, K. S.; Jang, Y. C.; Yeom, G. Y.; Lee, N. E. *Thin Solid Films* **2000**, *377*, 115–121.